

Influence of magnet eddy current on magnetization characteristics of variable flux memory machine

Hui Yang, Heyun Lin, Z. Q. Zhu, and Shukang Lyu

Citation: *AIP Advances* **8**, 056602 (2018);

View online: <https://doi.org/10.1063/1.5007785>

View Table of Contents: <http://aip.scitation.org/toc/adv/8/5>

Published by the [American Institute of Physics](#)

Articles you may be interested in

[A variable-mode stator consequent pole memory machine](#)

AIP Advances **8**, 056612 (2017); 10.1063/1.5007220

[Minimization of torque ripple in ferrite-assisted synchronous reluctance motors by using asymmetric stator](#)

AIP Advances **8**, 056606 (2017); 10.1063/1.5006114

[Magnetic and electron spin resonance studies of W doped \$\text{CoFe}_2\text{O}_4\$ polycrystalline materials](#)

AIP Advances **8**, 055801 (2017); 10.1063/1.5003826

[Tailoring of magnetic softness and GMI effect in Fe-rich thin magnetic wires](#)

AIP Advances **8**, 056102 (2017); 10.1063/1.5004701

[Damping constant measurement and inverse giant magnetoresistance in spintronic devices with \$\text{Fe}_4\text{N}\$](#)

AIP Advances **7**, 125303 (2017); 10.1063/1.4994972

[Analytical torque calculation and experimental verification of synchronous permanent magnet couplings with Halbach arrays](#)

AIP Advances **8**, 056609 (2017); 10.1063/1.5006731

HAVE YOU HEARD?

Employers hiring scientists and
engineers trust

PHYSICS TODAY | JOBS

www.physicstoday.org/jobs



Influence of magnet eddy current on magnetization characteristics of variable flux memory machine

Hui Yang,^{1,a} Heyun Lin,¹ Z. Q. Zhu,² and Shukang Lyu¹

¹*School of Electrical Engineering, Southeast University, Sipailou 2, 210096, Nanjing, China*

²*Department of Electronic and Electrical Engineering, University of Sheffield, Mappin Street, Sheffield S1 3JD, United Kingdom*

(Presented 7 November 2017; received 2 October 2017; accepted 20 October 2017; published online 5 December 2017)

In this paper, the magnet eddy current characteristics of a newly developed variable flux memory machine (VFMM) is investigated. Firstly, the machine structure, non-linear hysteresis characteristics and eddy current modeling of low coercive force magnet are described, respectively. Besides, the PM eddy current behaviors when applying the demagnetizing current pulses are unveiled and investigated. The mismatch of the required demagnetization currents between the cases with or without considering the magnet eddy current is identified. In addition, the influences of the magnet eddy current on the demagnetization effect of VFMM are analyzed. Finally, a prototype is manufactured and tested to verify the theoretical analyses. © 2017 Author(s). All article content, except where otherwise noted, is licensed under a Creative Commons Attribution (CC BY) license (<http://creativecommons.org/licenses/by/4.0/>). <https://doi.org/10.1063/1.5007785>

I. INTRODUCTION

Variable flux memory machines (VFMM) equipped with low coercive force (LCF) aluminum-nickel-cobalt (AlNiCo) magnets¹⁻⁴ are recognized as a viable candidate for wide-speed-range applications. The armature windings can energize a temporary d -axis magnetizing current pulse to enable online flux control with negligible excitation copper loss. VFMM can combine the distinct synergies of acceptable torque capability in low-speed operation and high efficiency in high-speed operation. Due to short duration of the demagnetizing current, the magnetic field intensity in permanent magnets (PM) varies dramatically, and hence significantly severe PM eddy current will be induced particularly under high-level demagnetization current transient. On the other hand, VFMMs usually employ AlNiCo PM, of which electric conductivity PM is much higher than neodymium-iron-boron (NdFeB) commonly used in the conventional PM machines.⁴ Meanwhile, the magnet eddy current analyses in VFMM remains unreported in existing literature. The purpose of this paper is therefore to fill this knowledge gap.

In this paper, the influence of the PM eddy current on the magnetization characteristics of VFMM is unveiled and analyzed. Fig. 1(a) shows the investigated VFMM machine topology, which is geometrically characterized by a hybrid PM structure. The 21-slot/4-pole fractional-slot distributed winding configuration is utilized to uniformize the magnetizing effect regardless of the rotor position. The triangle air-gap flux barriers are inset between two adjacent NdFeB PM segments to alleviate the armature demagnetization effect on AlNiCo PMs.

The flux regulation principle can be illustrated by the AlNiCo hysteresis model as shown in Fig. 1(b).^{3,4} The intersection of the load line and recoil line determines the operating point of AlNiCo PM, and its displacement on the H -axis is determined by the applied magnetomotive force (MMF). Thus, the specific operating point under different magnetization levels can be adjusted by calculating the remanence B_{rk} according to the temporary MMF. For instance, if point A is assumed to be the initial operating point. Once the demagnetizing current pulse is applied, the operating point will shift

^ahuiyang@seu.edu.cn

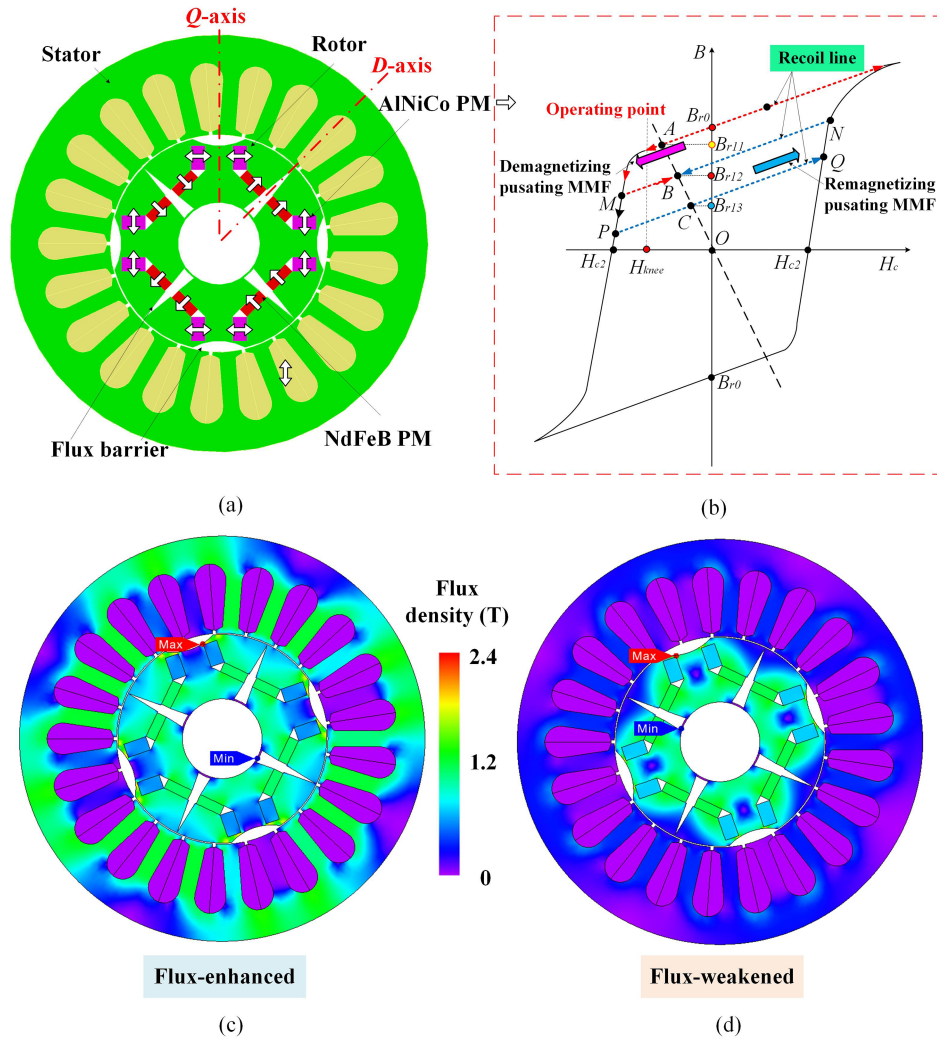


FIG. 1. (a) VFMM Topology. (b) Flux regulation principle. Open-circuit field distributions under (c) the flux-enhanced state and (d) the flux-weakened state.

along AMB and stabilize at B as a new operating point. If the starting working point is assumed as point C , the working point will track along $CQNB$ and terminate at B after a remagnetizing current pulse. As a result, the air-gap flux of the proposed VFMM can be flexibly adjusted by changing magnetization state of AlNiCo PMs online. The field distributions under different magnetization states are shown in Figs. 1(c) and (d), respectively. Here, we define “flux-enhanced” and “flux-weakened” states as the cases when the AlNiCo PMs are magnetized in the same or opposite directions with NdFeB PMs. The design parameters of the developed VFMM is listed in Table I, and JMAG 15 package is employed for finite element (FE) simulation.

TABLE I. Basic design parameters of VFMM.

Items	Parameters	Items	Parameters
Stator outer diameter (mm)	122	NdFeB PM thickness (mm)	2.5
Stator inner diameter (mm)	68	NdFeB PM width (mm)	9
Air-gap length (mm)	0.35	Magnet grade	N35SH/LMGT72
Rated current (Arms)	5	AlNiCo PM thickness (mm)	4
Active stack length (mm)	55	AlNiCo PM width (mm)	10

II. PM EDDY CURRENT MODELING

The governing magnetic field equations in consideration of magnet eddy current can be expressed as^{5,6}

$$\nabla \times \nu \nabla \times \mathbf{A} - \nabla \nu \nabla \cdot \mathbf{A} = \mathbf{J}_0 + \mathbf{J}_e + \nu \nabla \times \mathbf{M} \quad (1)$$

$$\mathbf{J}_e = -\sigma \left(\frac{\partial \mathbf{A}}{\partial t} + \nabla \phi \right) \quad (2)$$

$$\nabla \cdot \mathbf{J}_e = 0 \quad (3)$$

where \mathbf{J}_e and ν are the magnet eddy current density of AlNiCo PM, respectively; σ is the electrical conductivity of AlNiCo PM, which is approximately 1.6×10^6 S/m; \mathbf{A} is the vector magnetic potential, \mathbf{M} is the magnetizing intensity, \mathbf{J}_0 is the current density. ϕ is scalar magnetic potential function.

III. INFLUENCE OF MAGENT EDDY CURRENT ON MAGNETIZATION CHARACTERISTICS

A. PM eddy current behavior during magnetizing transient

The peak value and time duration of demagnetizing current pulse are initially set as 4.3A and 20ms. Five probed points along the central line of AlNiCo PM are shown in Fig. 2(a). Fig. 2(b) shows the variations of eddy current densities during the demagnetization transient. The eddy current density varies more dramatically for the cases when the PM segments are closer to the air-gap. This is mainly attributed to the existence of the iron bridge, where severe magnetic saturation occurs during the demagnetizing transient. Meanwhile, the eddy current densities of all five points peaks at around 3ms, and sharply drops to zero after 20ms.

B. Magnetization performance

When applying a *d*-axis current pulse with 4.3A and 20ms duration, the residual flux density with or without considering PM eddy current effect is shown in Fig. 3(a). Besides, the resultant residual flux density as a function of the demagnetizing current is plotted in Fig. 3(b). The magnet eddy current exerts an obstruction effect on the demagnetizing MMF. Consequently, the actual flux density during and after the demagnetization transient is higher than the ideal one without considering PM eddy current. As a result, it is necessary to correct the open-circuit back-electromotive force (EMF) versus demagnetizing current table by accounting for the PM eddy current effect.

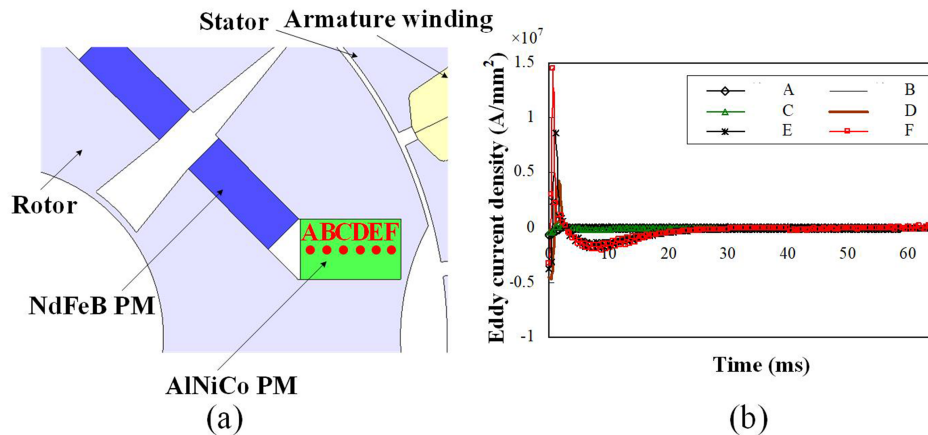


FIG. 2. The variations of the eddy current density of five probed PM points. (a) Probed points. (b) The eddy current density during the demagnetization process.

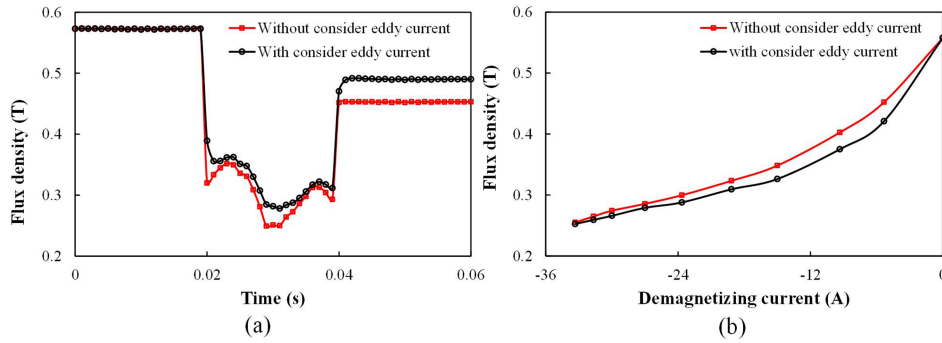


FIG. 3. (a) PM working point variation when applying a d -axis current pulse with 4.3A and 20ms. (b) The resultant residual flux density as a function of the demagnetizing current.

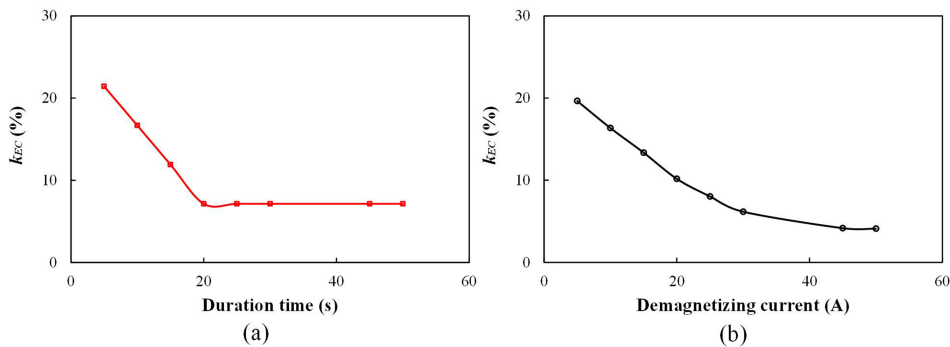


FIG. 4. The variations of k_{EC} with (a) time duration and (b) magnitude of the demagnetizing current pulse.

The result difference with or without considering LCF magnet eddy current effect can be defined by a coefficient k_{EC} , i.e.,

$$k_{EC} = \left| \frac{E_2 - E_1}{E_2} \right| \times 100\% \quad (4)$$

where E_1 and E_2 are the fundamental EMF magnitudes after demagnetization with or without considering the PM eddy current effect. The variations of k_{EC} with time duration and magnitude of the demagnetizing current are plotted in Fig. 4. The PM eddy current tends to show smallest impact on the demagnetization effect when the time duration exceeds 20ms, which can be explained by the PM eddy current density results as reflected in Fig. 2(b). Meanwhile, k_{EC} decreases steadily when the demagnetizing current reaches approximately 40A. This is mainly due to the counteract effect reduction of the magnet eddy current when the demagnetizing MMF is strong.

IV. EXPERIMENTAL VERIFICATION

A VFMM prototype is manufactured as shown in Fig. 5(a), which has a similar structure with the interior-PM machine, but with a relatively complicated rotor. The stator is similar to that of the conventional distributed-winding machine. In order to ease manufacture, the laminated rotor is linked at the inner shaft by 0.5-mm bridges, and the air barriers can be filled by non-magnetic material, such as the stainless steel 300 series. It should be noted that the magnetization control circuit is implemented based on a single-phase H bridge converter similar to the pulse-width-modulation (PWM) chopper. The duration of the magnetizing current is set as approximately 50ms in the experiment. The FE and test results of fundamental EMF magnitude with demagnetizing current pulse are shown in Fig. 5(b). The FE predictions accounting for the PM eddy current effect show greater agreement with the measurement.

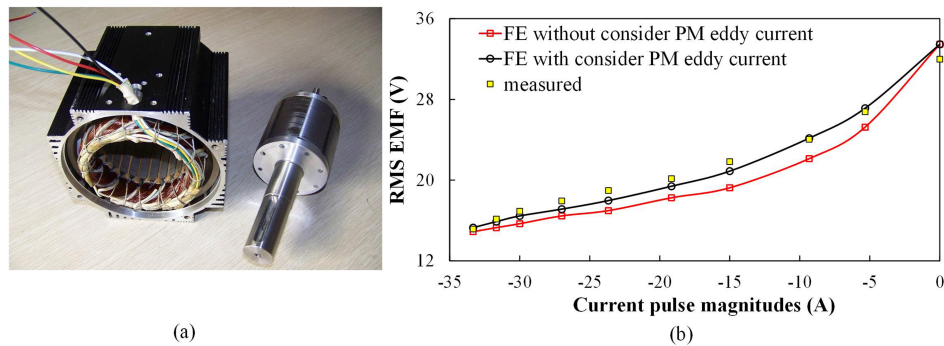


FIG. 5. (a) The prototype VFMM. (b) FE-predicted and measured back-EMFs as functions of demagnetizing currents.

V. CONCLUSION

In this paper, the effects of AlNiCo magnet eddy current on the magnetization characteristics of an emerged VFMM are investigated. The machine topology and flux regulation principle are described, respectively. The PM eddy current features during the demagnetization process are investigated. It can be found that the PM points closer to air gap experience a significant fluctuation of the eddy current density, and all the PM eddy current densities swiftly drops to zero when the time duration of the current pulse exceeds 20ms. Besides, the required demagnetization currents between the cases with or without considering the magnet eddy current differ more slightly when the duration and peak value of the demagnetizing current are set as higher than 20ms and 40A. Finally, the tests on a VFMM prototype have been carried out to validate the theoretical analyses.

ACKNOWLEDGMENTS

This work was jointly supported by National Natural Science Foundation of China (51707036 and 51377020), Specialized Research Fund for the Doctoral Program of Higher Education of China (20130092130005), Natural Science Foundation of Jiangsu Province for Youth (BK20170674), and the Fundamental Research Funds for the Central Universities (3216007453).

¹ V. Ostovic, *IEEE Ind. Appl. Mag.* **9**, 52 (2003).

² K. Sakai, K. Yuki, Y. Hashiba, N. Takahashi, and K. Yasui, in *Proc. Int. Conf. on Electr. Mach. Syst.* (Tokyo, Japan, 2009), pp. 1–6.

³ C. Yu, K. T. Chau, and J. Z. Jiang, *J. Appl. Phys.* **105**, 07F114 (2009).

⁴ H. Yang, H. Lin, S. Fang, Z. Q. Zhu, and Y. Huang, *IEEE Trans. Magn.* **50**, 8103904 (2014).

⁵ H. Polinder and M. Hoeijmakers, *J. IEE Proc. Electr. Power Appl.* **146**, 261 (1999).

⁶ J. Ji, J. Luo, Q. Lei *et al.*, *AIP Advances* **7**, 056646 (2017).